Supporting Information

Indolo[3,2-b]carbazole-based hyper-cross-linked polymers for blue-light-driven selective organic sulfide oxidation in water

Si-Jia Wang, Zhou-Rui Yan, Zi-Yi Zhao, Jin-Peng Liu, Fan Li, Guoliang Liu*, and Lin-Bing Sun*

State Key Laboratory of Materials-Oriented Chemical Engineering, Jiangsu National Synergetic Innovation Center for Advanced Materials (SICAM), College of Chemical Engineering, Nanjing Tech University, Nanjing 211816, China

*Corresponding authors. E-mail: glliu@njtech.edu.cn; lbsun@njtech.edu.cn.

1. Chemicals and reagents

The chemical anhydrous aluminum trichloride (≥99.0%, Greagent), tetrabutylammonium iodide (n-Bu_4NI, ≥99.0%, Adamas), benzaldehyde (≥99.0%, Adamas), 1-Bromohexane (≥99.0%, Adamas), indole (≥99.0%, Adamas), 3,3',5,5'-tetramethylbenzidine (TMB，≥99.0%, Adamas), iodine (I_2, ≥99.0%, Adamas), 1,3,5-tris(bromomethyl)benzene (TBMB, ≥99.0%, TCI), 1,3,5-tris(brommethyl)-2,4,6-trimethylbenzol (TBMTB, ≥99.0%, TCI), Sodium hydroxide (NaOH, ≥99.0%, Adamas), fluoroboric acid (HBF_4, 48wt.% in water, Sigma-Aldrich), potassium bromide (IR grade for spectroscopy, 99+%, Acros), deuterated dimethyl sulfoxide (DMSO-d_6, 99.9%D+0.03%TMS, Adamas) were purchased from corresponding suppliers. Deionized water (homemade), tetrahydrofuran (THF), acetone, acetonitrile (MeCN), N, N-dimethylformamide (DMF), 37% concentrated hydrochloric acid (HCl), dichloromethane (DCM), and methanol (MeOH) were purchased as regent grade from Sinopharm Chemical Reagent Shanghai Co., Ltd.. All reagents and solvents used in synthetic studies were commercially available and used as supplied without further purification.

2. Experimental Methods

2.1 Synthesis of 5,11-dihexyl-6,12-diphenyl-5,11-dihydroindolo[3,2-b]carbazole

Synthesis of 5,11-dihexyl-6,12-diphenyl-5,11-dihydroindolo[3,2-b]carbazole was carried out as shown in Scheme 1. Benzaldehyde (1.06 g, 10 mmol), indole (1.17 g, 10 mmol) and acetonitrile (27 mL) were added to a round-bottomed flask and stirred until clarified. Another tetrabutylammonium iodide (0.37 g, 1 mmol) and tetrafluoroboric acid (0.16 mL, 1 mol) were dissolved in acetonitrile (3 mL) and slowly added dropwise to the above solution under an ice bath. The mixture was reacted for 48 h at room temperature and then filtered, the solid was washed with acetonitrile and methanol respectively, and dried in vacuum at 60 ^oC to obtain the intermediate M1.

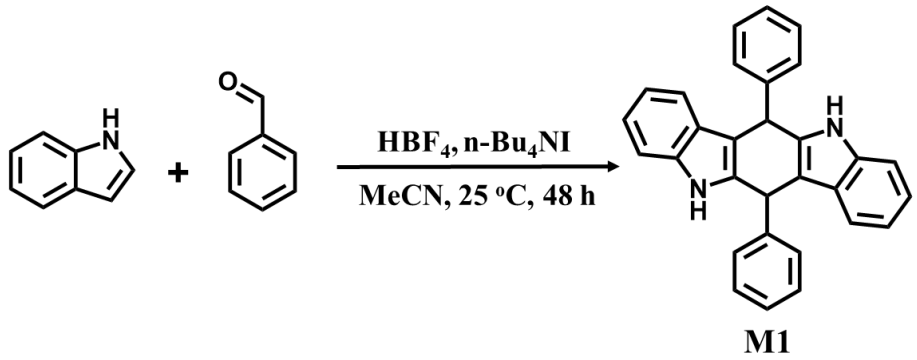

Scheme S1. The synthetic route of M1.

M1 (1 g, 2.43 mmol), NaOH (0.5 g, 12.5 mmol) and DMF (30 mL) were added to a round-bottomed flask and stirred under nitrogen protection for 30 min. 1-Bromohexane (1.37 mL, 9.75 mmol) was added dropwise and the reaction was carried out at room temperature for 15 h. Add 50% ethanol (60 mL) and continue stirring for 1 h. Filtered, ethanol washed and the solid was dried in vacuum at 60 °C to give M2.

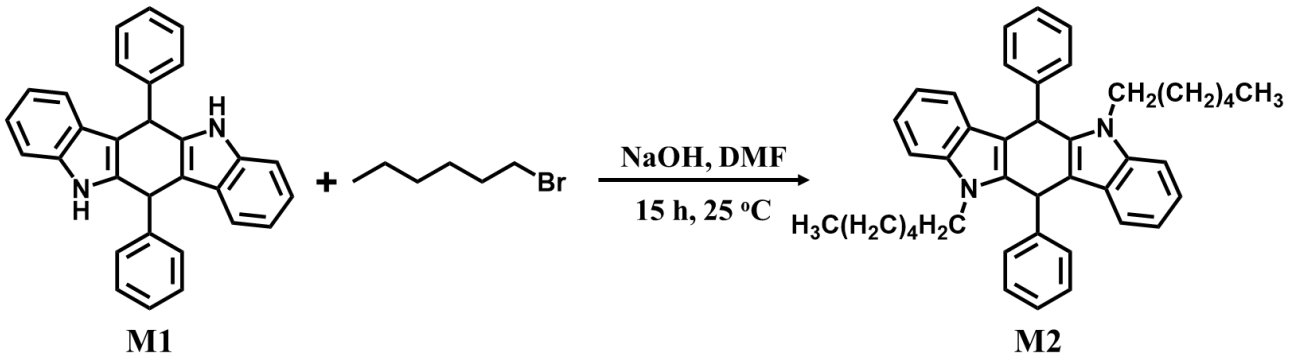

Scheme S2. The synthetic route of M2.

M2 (1 g, 1.73 mmol) was added to a round bottom flask with an appropriate amount of DMF, and then I_2 (0.88 g, 3.46 mmol) was added and the reaction was carried out at 170 °C for 4 h. At the end of the reaction, the mixture was cooled in a refrigerator and a yellow solid was precipitated. The solid was filtered and washed with cold DMF and dried to give the ICZ monomer 5,11-dihexyl-6,12-diphenyl-5,11-dihydroindolo[3,2-b]carbazole. The reaction process was monitored by ^{1}H NMR.The purity of ICZ monomers was detected by ^{1}H NMR, as shown in **Fig. S1**. ^{1}H NMR (400 MHz, DMSO)

δ 7.74 - 7.64 (m, 10H), 7.42 (d, J = 8.2 Hz, 2H), 7.35 - 7.26 (m, 2H), 6.76 (t, J = 7.5 Hz, 2H), 6.36 (d, J = 7.9 Hz, 2H), 1.60 - 1.34 (m, 4H), 1.26 - 1.08 (m, 16H), 0.84 (q, J = 7.9 Hz, 6H).

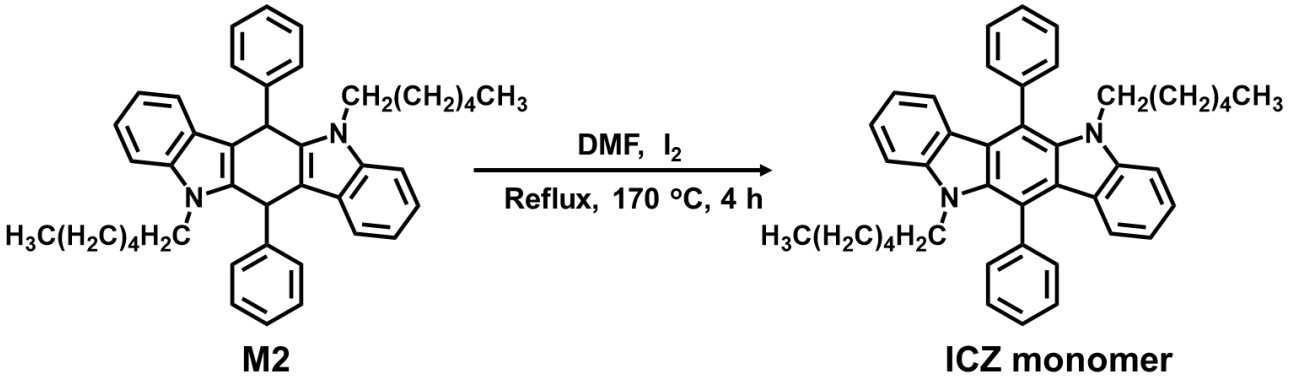

M2 ICZ monomer

Scheme S3. The synthetic route of 5,11-dihexyl-6,12-diphenyl-5,11-dihydroindolo[3,2-b]carbazole.

2.2 Singlet oxygen monitoring test

Weigh 15 mg of TMB and dissolve it in a 3 mL mixture of water and tetrahydrofuran. Add 5 mg of catalyst. Illuminate with 420 nm light for 1 min. Measure the UV-visible absorbance of the two catalysts using UV-Vis DRS, and subsequently measure the absorbance change every 2 min.

2.3 Characterizations

^{1}H NMR and ^{13}C NMR spectra were recorded at room temperature on a Bruker Avance 400 MHz spectrometer. Chemical shifts are given in ppm with respect to TMS. The rotational speed was set as 12 kHz and the scanning time was 1 h. Fourier transform infrared (FT-IR) spectra were recorded on KBr (1:30, w/w) pellets in the 4000-600 cm^{-1} range using a Perkin-Elmer Spectrum One FT-IR spectrometer. UV-Visible diffuse reflectance spectra (UV-Vis DRS) were performed on Shimadzu UV-3600 PLUS and the test range is from 200 to 800 nm using $BaSO_4$ as a reference. N_2 adsorption-desorption isotherms were measured using BELSORP-MINI analyzer at 77 K. The samples were degassed at 150 ^{o}C for 12 h prior to analysis. The Brunauer-Emmett-Teller (BET) surface area was calculated using adsorption data in a relative pressure ranging from 0.05 to 0.30. The pore diameter

was calculated from the adsorption branch by using the no-local density functional theory (NLDFT) method. Thermogravimetric analysis (TGA) curves were obtained by use of a thermobalance (STA-499C, NETZSCH). The sample was heated from room temperature to 800 °C with a heating rate of 5 °C·min^{-1} under a flow of N_2 (20 mL·min^{-1}). Powder X-ray diffraction (PXRD) patterns were collected on a Bruker D8 Avance S5 diffractometer with Cu Kα radiation at 40 kV and 40 mA. The elements and chemical bonds on the surface of the prepared material were measured using X-ray photoelectron spectroscopy (XPS, Thermo Scientific K-Alpha, USA). Photoluminescence spectra and luminescence decay was measured on a HORIBA FluoroLog-3 fluorescence spectrometer. Scanning Electron Microscopy (SEM) experiments were carried out on a Hitachi Regulus8100 at 3 kV equipped with an energy dispersive spectrometer (EDS, Oxford Instruments, 80 mm2 detector). Samples were treated via Pt sputtering before observation. The electron paramagnetic resonance (EPR) experiments were conducted on an electron paramagnetic resonance spectrometer (JEOL, JES-FA300).

Electrochemical performance tests were performed on a CHI730E electrochemical workstation. 10 mg of catalyst sample was dispersed in 400 μL of ethanol, followed by the addition of 40 μL of Nafion reagent. The mixture was sonicated for 30 min to make the dispersion homogeneous. The dispersed mixture was added dropwise onto an FTO glass and allowed to dry at room temperature for photoelectric testing. The test was performed using aqueous sodium sulfate solution as the electrolyte, Pt electrode as the counter electrode, Ag/AgCl as the reference electrode, and 420 nm visible light as the light source. The photocurrent test light interval was 30 s and more than 4 test cycles. Photoelectrochemical measurements were performed on an electrochemical workstation (CHI 660E, CH Instruments Inc., Shanghai) in a standard three-electrode system. The photocatalyst-coated glassy carbon (Φ = 3 cm) was chosen as the working electrode, an Ag/AgCl electrode was applied as a reference electrode, and Pt wire was used as the counter electrode. The electrolyte is a 0.1 M Na_2SO_4 aqueous solution. The samples (10 mg) were dispersed into 1 mL ethanol with 50 μL Nafion mixed

solution, and the working electrode was prepared by dropping the suspension onto the surface of the glassy carbon electrode and drying repeatedly (10 μL × 15). The photocurrents were recorded under the 420 nm LED light switching every 20 seconds and 0.5 M Na_2SO_4 solution was chosen as a primer. Electrochemical impedance spectroscopy (EIS) measurement was performed in the range of 0.1 Hz100 KHz without light irradiation and the electrolyte was 2.5 mM potassium solution. The ZSimpWin software was used to fit the equivalent circuit of EIS. Mott-Schottky analysis was executed at the frequency of 1000 Hz and the potential range was set between -1 and 1 V on the basis of 0.5 M Na_2SO_4 solution. Photoluminescence (PL) spectra were measured on a PE8500 fluorescence spectrophotometer.

3. Additional Figures

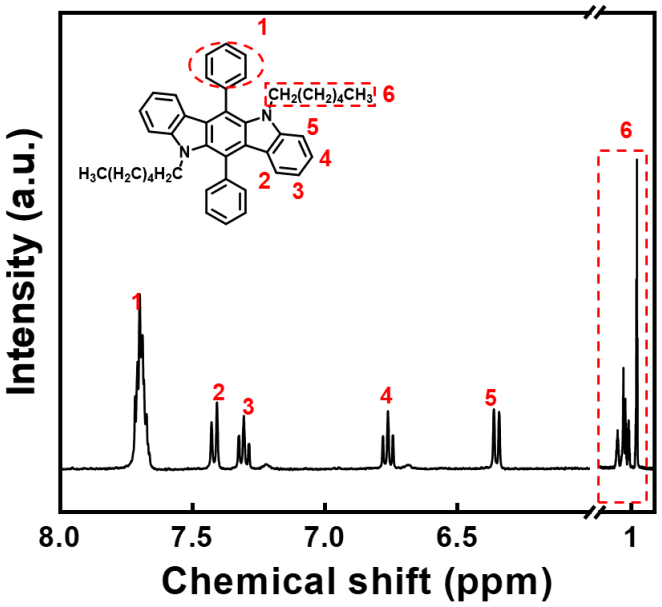

Fig. S1 ^{1}H NMR analysis of 5,11-dihexyl-6,12-diphenyl-5,11-dihydroindolo[3,2-b]carbazole.

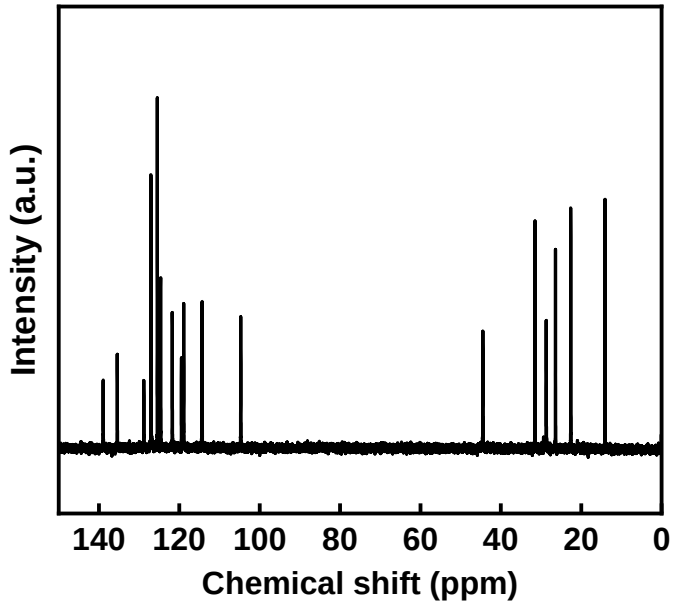

Fig. S2 ^{13}C NMR analysis of 5,11-dihexyl-6,12-diphenyl-5,11-dihydroindolo[3,2-b]carbazole.

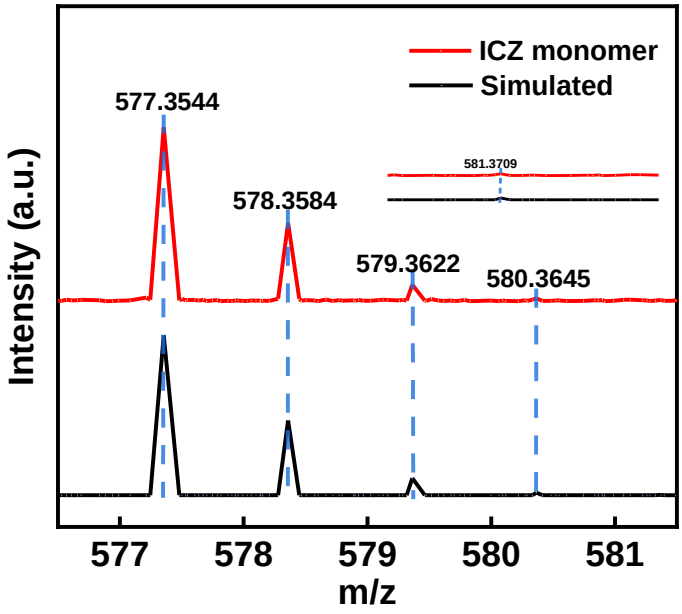

Fig. S3 HRMS analysis of 5,11-dihexyl-6,12-diphenyl-5,11-dihydroindolo[3,2-b]carbazole.

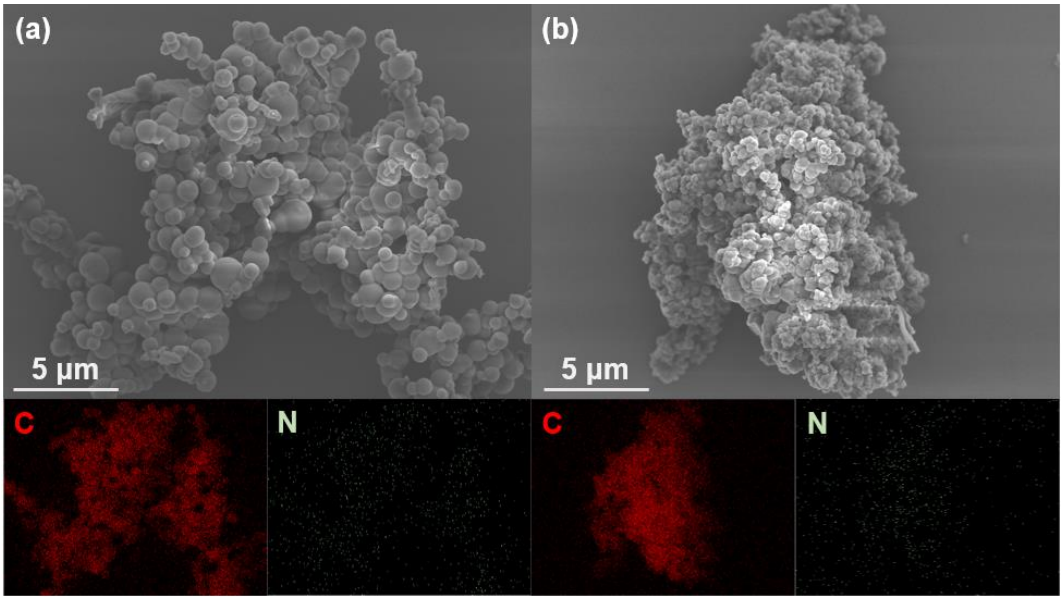

Fig. S4 SEM images and EDS elemental distribution of C and N elements of (a) NUT-19 and (b) NUT-19-Me.

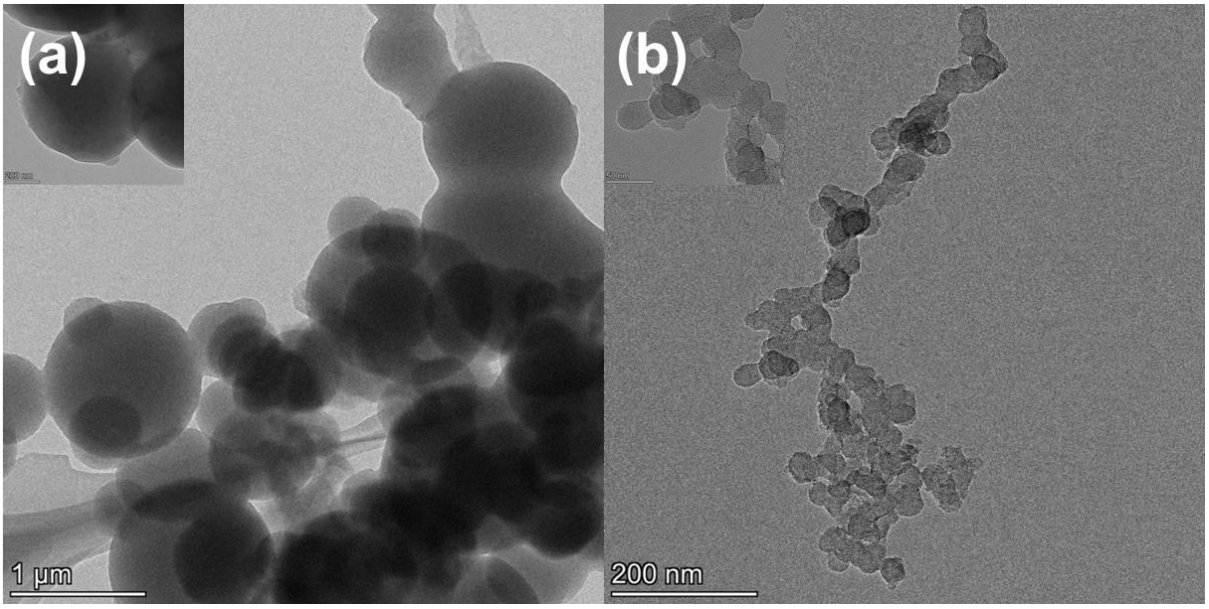

Fig. S5 TEM images of (a) NUT-19 and (b) NUT-19-Me.

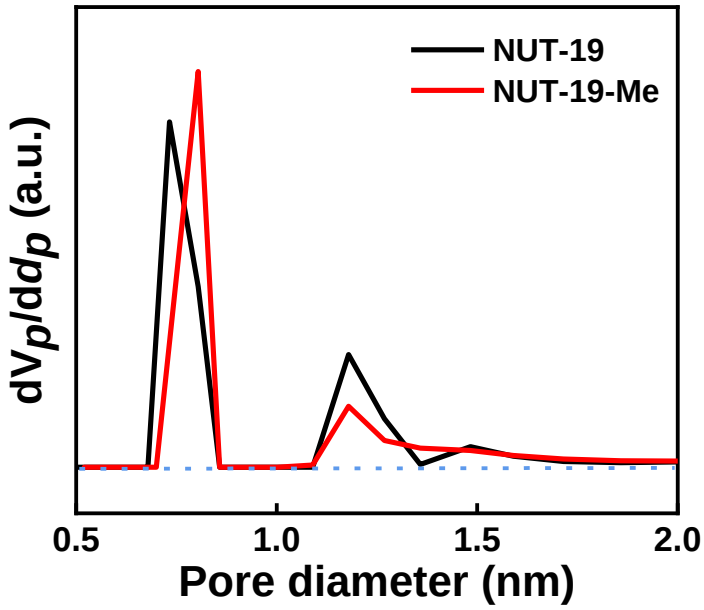

Fig. S6 NLDFT pore size distribution of NUT-19 and NUT-19-Me.

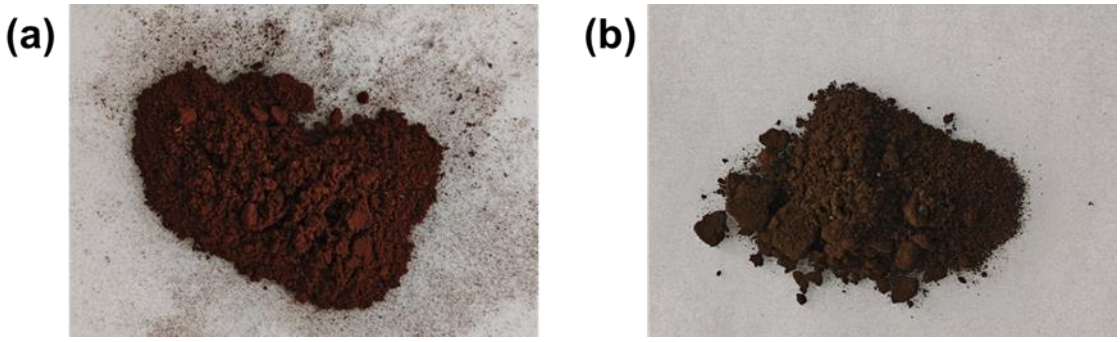

Fig. S7 Photograph images of (a) NUT-19 and (b) NUT-19-Me.

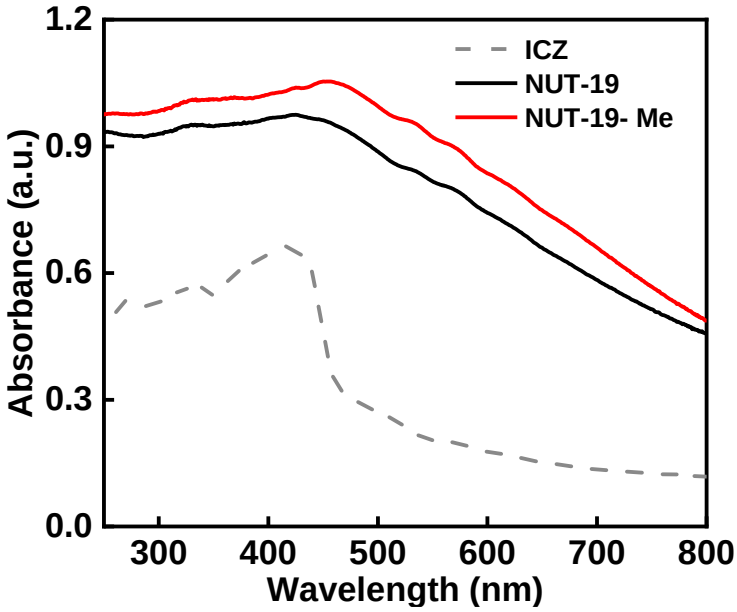

Fig. S8 UV-vis DRS of ICZ, NUT-19 and NUT-19-Me.

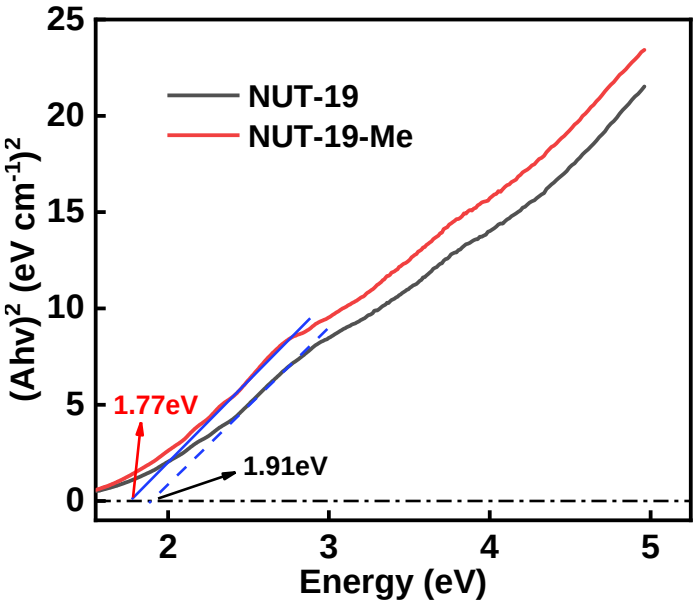

Fig. S9 Tauc plots of NUT-19 and NUT-19-Me.

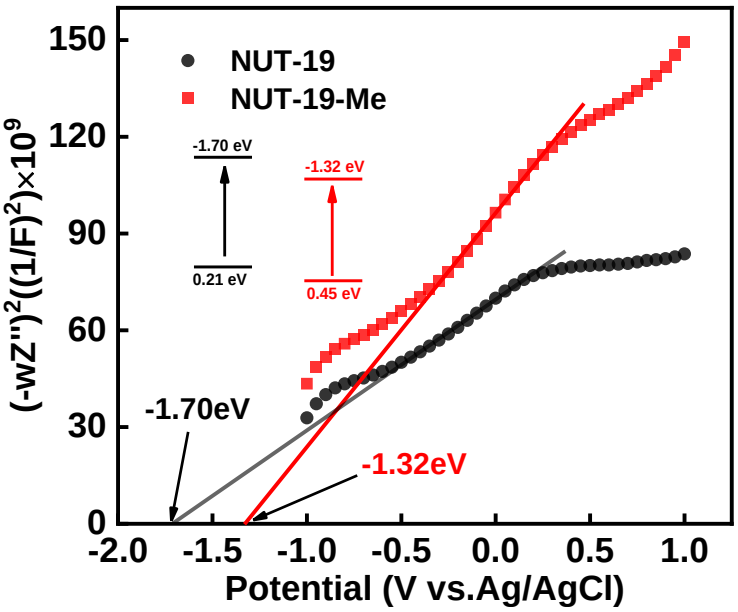

Fig. S10 Mott-Schottky plots of samples and the determined energy levels of LUMO and HOMO for NUT-19 and NUT-19-Me.

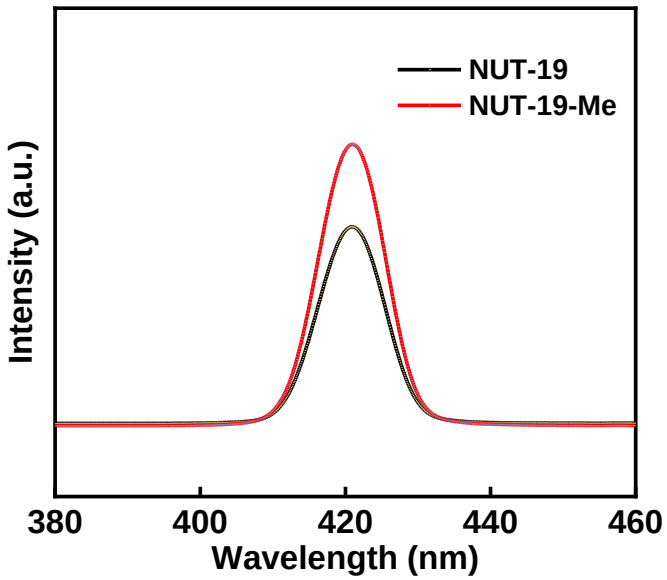

Fig. S11 PL spectra of NUT-19 and NUT-19-Me.

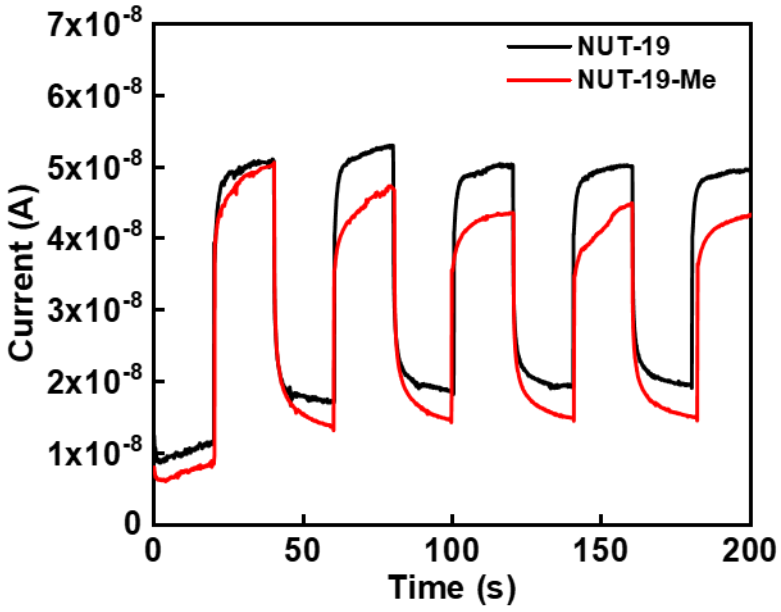

Fig. S12 Transient photocurrent responses of NUT-19 and NUT-19-Me.

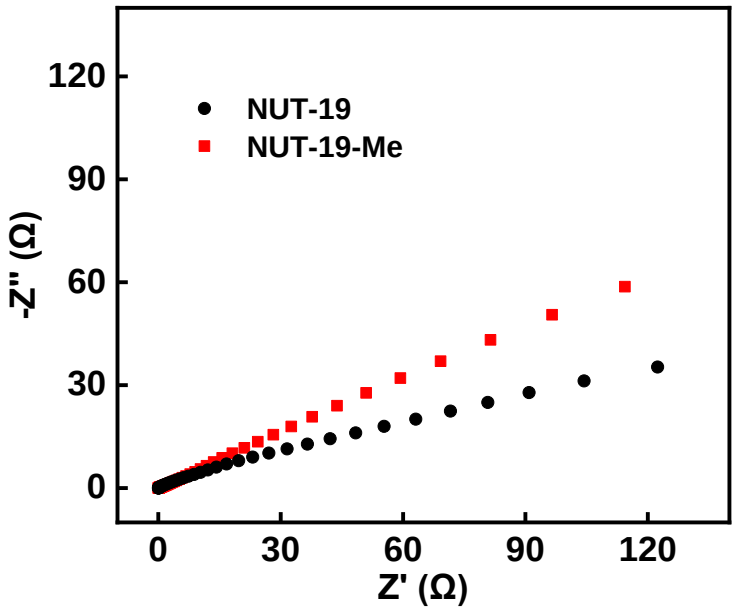

Fig. S13 EIS of NUT-19 and NUT-19-Me.

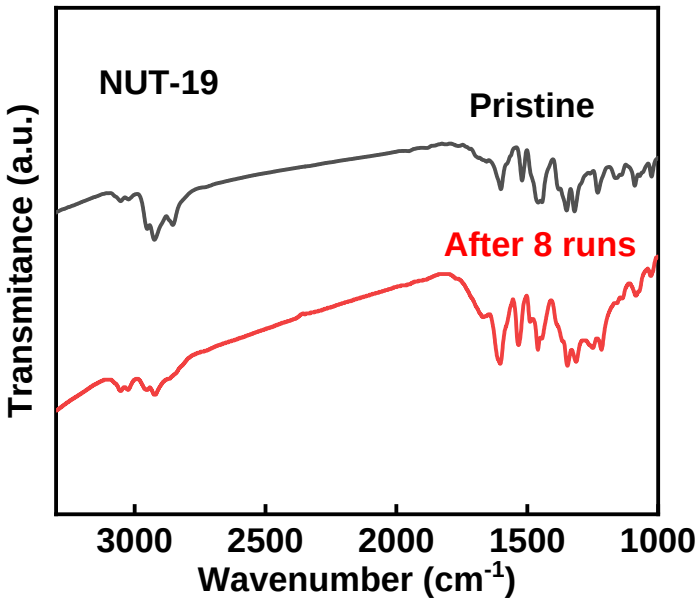

Fig. S14 FT-IR analysis of NUT-19 after performance evaluation for 8 runs.

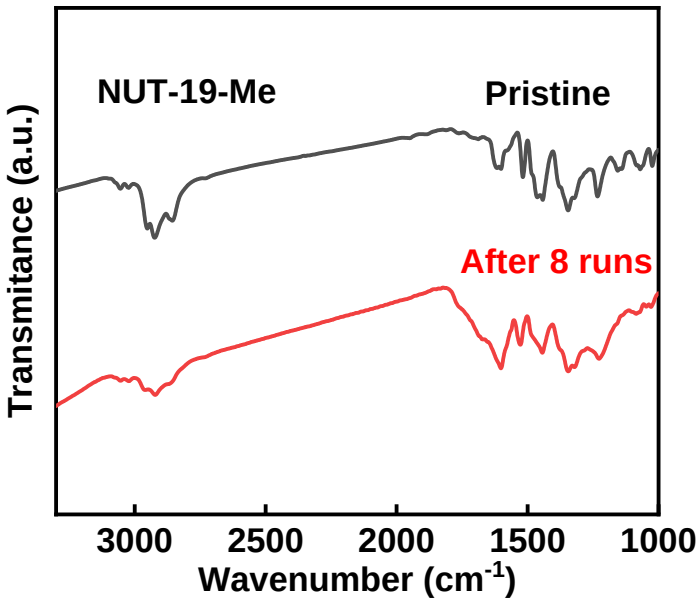

Fig. S15 FT-IR analysis of NUT-19-Me after performance evaluation for 8 runs.

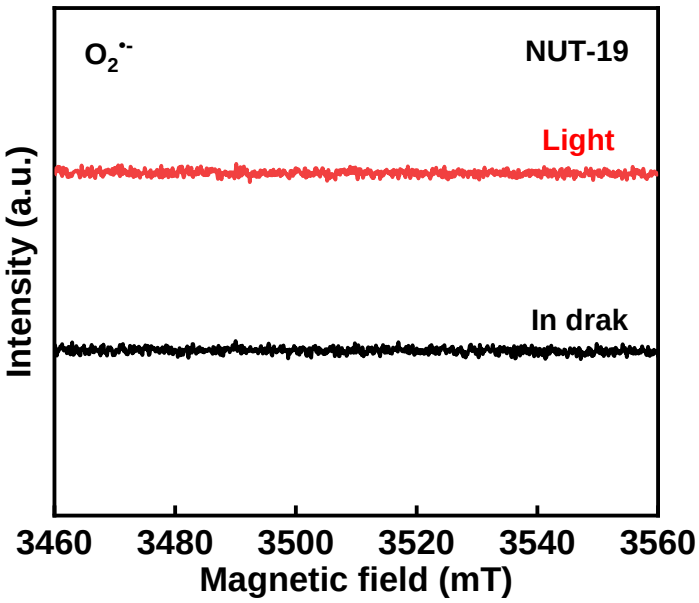

Fig. S16 EPR signals of DMPO capturing $O_2^{\bullet-}$ signals with time of light on NUT-19.

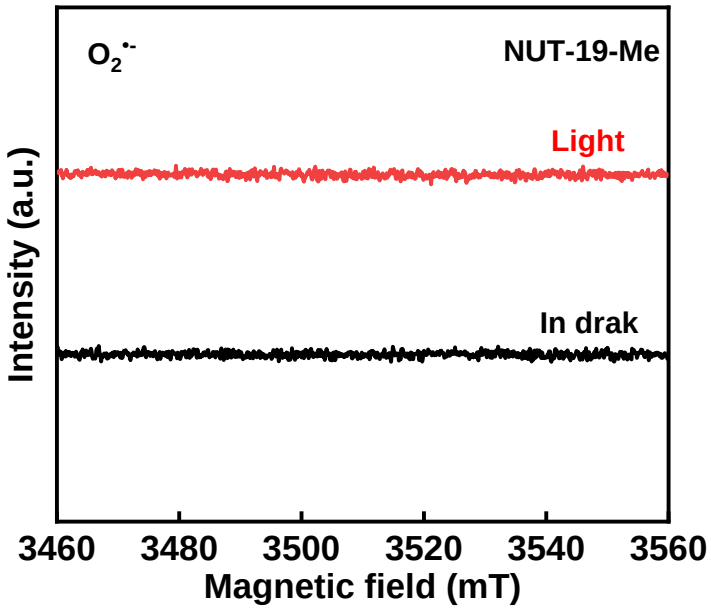

Fig. S17 EPR signals of DMPO capturing $O_2^{\bullet-}$ signals with time of light on NUT-19-Me.

Table S1. Conversion of thioanisole at different wavelengths and intensities of light over the photocatalyst NUT-19.

Wavelength (nm)	**Power density (mW/cm^2)**	**Conversion (%)**
Black	0	0
420	40	59
420	80	80
420	120	99
Red light (630-660)	120	58
Sunlight (400-830)	120	74

Table S2. Comparison of the photocatalytic performance of NUT-19 and NUT-19-Me with reported materials.

Photocatalyst	Conditions	T (h)	Yield (%)	Ref.
CMP-BDD	HCl, O_2, 14 W blue LED, RT	24	>99	1
TCPP-CMP	CH_3CN/ H_2O, O_2 (1 atm), 100 W white LED, 25 ^oC	16	>99	2
BN@TTCOP	Methanol, O_2 (1 atm), white LED lamp, RT	7	>99	3
PyPor-COF	H_2O, Red LEDs (5 W,660 nm), RT	24	99	4
4F-COF	CH_3CN + MeOH,, O_2 (~0.1 MPa), 14 W LED lamp (0.20 W/cm^2), RT = 25 ± 2 ^oC	12	100	5
I-POP	MeOH, Red LEDs (5 W, 660 nm), RT	10	97	6
UNLPF-10 (0.1 mol%)	MeOH, air, blue LED, RT	8	99	7
PC-1(0.5)	MeCN, air, blue LED(456 nm), RT	18	79	8
$Cs_3Bi_2Br_9/TiO_2$	MeCN, air, blue LED(50 W), RT	24	86	9
Ir-Zr MOF	CH_3CN, O_2, blue LED(100 W), RT	18	79	10
NUT-19	H_2O, 20 W 420 nm LED, Air, 120 mW/cm^2	8	99	This work
NUT-19-Me	H_2O, 20 W 420 nm LED, Air, 120 mW/cm^2	11	98	This work

The power density for substrate expansion and cycling tests is 120 mW/cm^2.

References

1 H. Zhang, Q. Huang, W. Zhang, C. Pan, J. Wang, C. Ai, J. Tang, G. Yu, Benzodithiophenedione-based conjugated microporous polymer catalysts for aerobic oxidation reactions driven by visible-light, *ChemPhotoChem*, 2019, **8**, 645-651.

2 J. Jiang, Z. Liang, X. Xiong, X. Zhou, H. Ji, A carbazolyl porphyrin-based conjugated microporous polymer for metal-free photocatalytic aerobic oxidation reactions, *ChemCatChem*, 2020, **13**, 3523-3529.

3 X. Lan, Q. Li, Y. Zhang, Q. Li, L. Ricardez-Sandoval, G. Bai, Engineering donor-acceptor conjugated organic polymers with boron nitride to enhance photocatalytic performance towards visible-light-driven metal-free selective oxidation of sulfides, *Appl. Catal. B: Environ.*, 2020, **277**, 119274.

4 K.-K. Niu, T.-X. Luan, J. Cui, H. Liu, L.-B. Xing, P.-Z. Li, Red-light-based effective photocatalysis of a photosensitive covalent organic framework triggered singlet oxygen, *ACS Catal.*, 2024, **4**, 2631-2641.

5 Q. Xie, A. Chen, Z. Gao, S. Gu, B. Wei, R. Liang, F. Zhang, Y. Zhao, J. Tang, C. Pan, G. Yu, Regulating conformational locking in covalent organic framework for selective and recyclable photocatalytic transformation, *Small*, 2024, **48**, 2405550.

6 R. Paul, P. Kalita, D. Q. Dao, I. Mondal, B. Boro, J. Mondal, Linker independent regioselective protonation triggered detoxification of sulfur mustards with smart porous organic photopolymer, *Small*, 2023, **34**, 2302045.

7 J. A. Johnson, X. Zhang, T. C. Reeson, Y.-S. Chen, J. Zhang, Facile control of the charge density and photocatalytic activity of an anionic Indium porphyrin framework via in situ metalation, *J. Am. Chem. Soc.*, 2014, **45**, 15881-15884.

8 S. K. Serviou, P. L. Gkizis, D. P. Sánchez, N. Plassais, F. Gohier, C. Cabanetos, C. G. Kokotos, Expanding the Use of benzothioxanthene imides to photochemistry: eco-friendly aerobic oxidation of sulfides to sulfoxides, *ChemSusChem*, 2024, **23**, e202400903.

9 Y. Zheng, H. Zhu, X. Xie, L. Yang, Q. Fan, Z. Le, Z. Xie, Lead-free perovskite $Cs_3Bi_2Br_9/TiO_2$ composites for atmospheric photocatalytic oxidation of sulfides, *Green Chem.*, 2024, **12**, 7031-7037.

10 L.-Q. Wei, B.-H. Ye, Cyclometalated Ir–Zr metal–organic frameworks as recyclable visible-light photocatalysts for sulfide oxidation into sulfoxide in water, *ACS Appl. Mater. Interfaces*, 2019, **44**, 41448-41457.